A Tonotopic Regulatory Axis Governing Isoform-Specific MYO7A Expression in Cochlear Hair Cells

Sihan Li [1], Sujin Jun [6, 7, 9, 10, 12], Yeri Kim [8, 11], Ayathi Gogineni [1], Franklin Lee [1], Chul Hoon Kim [13], Un-Kyung Kim [7, 9, 10, 12], Anthony W. Peng [6], Jung-Bum Shin[1 ,3, 4, 5, #]

Departments of Neuroscience[1], Biochemistry and Molecular Genetics[2], Cell Biology[3], Membrane and Cell Physiology[4], Otolaryngology[5], School of Medicine, University of Virginia, Charlottesville, VA 22903, USA

[6]Department of Physiology and Biophysics, University of Colorado Anschutz Medical Campus, Aurora, CO

Department of Biology[7], Immunology[8], Advanced Bio-Resource Research Center[9], School of Life Sciences[10], School of Medicine[11], BK21 plus KNU Creative BioResearch Group[12], Kyungpook National University, Daegu, Republic of Korea

[13]Department of Pharmacology, BK21 PLUS Project for Medical Science, Brain Research Institute, Yonsei University College of Medicine, 03722, Seoul, Korea.

[#] Corresponding authors

1. Abstract

Myo7a, a gene mutated in Usher syndrome and non-syndromic deafness, encodes an unconventional myosin essential for hair cell function. Our previous work revealed that cochlear hair cells express distinct *Myo7a* isoforms with distinct spatial and cell type-specific patterns. The canonical isoform (*Myo7a-C*) and a novel isoform (*Myo7a-N*) are co-expressed in outer hair cells (OHCs) but exhibit opposing tonotopic gradients, while inner hair cells (IHCs) primarily express *Myo7a-C*. These isoforms arise from distinct transcriptional start sites, indicating separate regulatory inputs. Here, we identify an intronic cis-regulatory element, *EnhancerA*, essential for tonotopically graded *Myo7a* expression. *EnhancerA* deletion reduces MYO7A protein levels, disrupts hair bundle morphogenesis, alters OHC mechanotransduction, and leads to hair cell degeneration and hearing loss. We further identify SIX2, a tonotopically expressed transcription factor that may interact with *EnhancerA* to regulate *Myo7a-N* in OHCs. These findings define a cis-trans regulatory axis critical for isoform-specific *Myo7a* expression and cochlear function.

2. Introduction

Sensory hair cells of the inner ear rely on the unconventional myosin motor protein MYO7A for proper development[1–3], maintenance of hair bundles[4,5], and mechanotransduction[6]. Loss-of-function mutations in the *Myo7a* gene cause both syndromic and non-syndromic forms of hereditary hearing loss. Notably, mutations in *MYO7A* underlie Usher syndrome type 1B, a disorder characterized by congenital

deafness, vestibular dysfunction, and progressive vision loss[1,7,8]. In non-syndromic cases, *Myo7a* mutations account for a significant proportion of autosomal recessive deafness[9,10] Given its central role in auditory function, MYO7A has emerged as a key target for inner ear gene therapy.

Previous studies have identified several *cis*-regulatory elements near the *Myo7a* locus[11,12], including a proximal promoter located upstream of the canonical transcriptional start site[6,11]. This promoter has been incorporated into gene therapy vectors and can drive robust expression in inner hair cells (IHCs). However, its activity in outer hair cells (OHCs) is weak or inconsistent, limiting its effectiveness for pan-hair cell targeting[13,14]. Regulatory sequences derived from non-mammalian species, such as conserved elements in zebrafish[12], have demonstrated hair cell-specific activity in transgenic models, but their correspondence to mammalian regulatory mechanisms and isoforms remains poorly understood.

Our previous work revealed that multiple *Myo7a* isoforms are expressed in cochlear hair cells, exhibiting distinct cell type-specific and tonotopic distributions[6]. The canonical isoform (*Myo7a-C*) and a novel isoform (*Myo7a-N*) are both expressed in OHCs, but exhibit opposing gradients along the cochlear tonotopic axis: *Myo7a-N* expression increases toward the cochlear base, while *Myo7a-C* is enriched toward the apex[15]. In contrast, IHCs primarily express *Myo7a-C* and low levels of *Myo7a-N.* These isoforms arise from separate transcriptional start sites[15], suggesting differential promoter usage and distinct trans-regulatory controls.

Here, we identify a previously uncharacterized intronic enhancer, *EnhancerA*, that is essential for tonotopically graded expression of *Myo7a* isoforms in both IHCs and OHCs. Deletion of *EnhancerA* leads to a progressive loss of MYO7A protein toward the cochlear base, impaired hair bundle morphogenesis, altered mechanotransduction, hair cell degeneration, and hearing loss. We further identify SIX2, a transcription factor with tonotopically graded expression, as a potential trans-regulator that interacts with *EnhancerA* to selectively control *Myo7a-N* expression in OHCs. Loss of SIX2 disrupts *Myo7a-N* expression, leads to disorganization of OHCs, and causes progressive auditory dysfunction. Together, these findings define a previously unrecognized *cis-trans* regulatory axis that governs spatial and isoform-specific expression of *Myo7a* in the cochlea and highlight new molecular mechanisms essential for hair cell function and therapeutic intervention.

3. Result

3.1. *EnhancerA* is required for tonotopically graded expression of *Myo7a*

We previously showed that *Myo7a* is expressed in multiple isoforms within the cochlea, each exhibiting distinct tonotopic expression patterns. Importantly, these isoforms are generated with different transcriptional start sites[15] (**Fig. 1A**), suggesting that their regulation may involve distinct combinations of *cis*- and *trans*-acting elements. Previous studies have identified multiple enhancers and promoters of *Myo7a*, yet none have been shown to support broad and robust expression across all cochlear hair cells[13,14]. We therefore hypothesized that additional regulatory elements may contribute to

the spatially patterned and cell type–specific expression of *Myo7a*.

To identify such elements, we reanalyzed publicly available ATAC-seq datasets from purified cochlear hair cells and supporting cells[16]. This analysis revealed a prominent, hair cell–specific peak of chromatin accessibility located within the third intron of the *Myo7a* gene, approximately 400 bp in length (**Fig. 1A,** genomic location provided in the figure legend). This peak represented the most accessible chromatin region within a 1Mb window surrounding *Myo7a*, consistent with a potential regulatory function. We designated this element *EnhancerA*.

To assess its functional role *in vivo*, we generated a mouse line harboring a 399 bp deletion targeting *EnhancerA* (Δ*EnhancerA* mice). Quantitative PCR analysis of cochlear cDNA from postnatal day 0 (P0) Δ*EnhancerA* mice revealed significantly reduced expression of all known *Myo7a* isoforms relative to wild-type (WT) controls, indicating that *EnhancerA* is essential for robust *Myo7a* transcription but not selective to *Myo7a* isoforms (**Fig. 1B**).

Strikingly, immunofluorescence analysis of MYO7A protein levels in Δ*EnhancerA* mice at P7 revealed a pronounced and spatially patterned reduction in both IHCs and OHCs (**Fig. 1C,** quantified for IHCs and OHCs in **Fig. 1D, E**). In the basal cochlea, MYO7A protein was nearly undetectable, indicating a severe transcriptional or post-transcriptional deficit. In contrast, the apical cochlear region retained robust MYO7A expression, though levels were reduced by approximately 50% compared to WT controls. This progressive, base-to-apex gradient of protein loss was consistently observed in OHCs, and to a slightly lesser extent, also in IHCs, establishing *EnhancerA* as a key *cis*-regulatory element that integrates spatial information along the cochlear axis to support robust and graded MYO7A expression, in a manner that does not discriminate between isoforms.

3.2. *EnhancerA* deletion impairs hair bundle development

To evaluate the developmental consequences of *EnhancerA* deletion, we performed scanning electron microscopy (SEM) on Δ*EnhancerA* cochleae at P7, a stage when hair bundle maturation is largely complete. In the most basal cochlear region, where MYO7A loss was the most severe, we observed marked disorganization of hair bundles in both IHCs and OHCs (**Fig. 2A, B**). Defects included the near-complete absence of the shortest row of stereocilia, a reduced number of middle and tallest row stereocilia, and disorganized stereocilia clusters. The clustering phenotype suggests impaired formation or maintenance of interstereociliary links, a process dependent on MYO7A function.

In contrast, hair cells in more apical regions, where residual MYO7A protein remained, displayed largely normal bundle morphology resembling that of WT controls (**Fig. 2A**). These findings indicate that *EnhancerA* is required for proper stereocilia development in a spatially graded manner and that even substantially reduced MYO7A expression is sufficient to support bundle formation in the mid-basal regions of the

cochlea.

3.3. Hair cell loss and hearing loss in Δ*EnhancerA* mice

To determine whether these structural defects lead to auditory dysfunction, we measured auditory brainstem responses (ABRs) and distortion product otoacoustic emissions (DPOAEs). At 3 weeks of age, Δ*EnhancerA* mice exhibited mild to moderate hearing loss, particularly at mid-to-high frequencies (**Fig. 2C**), consistent with the basal-to-apical gradient of MYO7A depletion. Distortion product otoacoustic emissions (DPOAEs) were largely unaffected at this stage. However, by 8 weeks, Δ*EnhancerA* mice exhibited profound hearing loss across all frequencies, accompanied by the near-complete loss of DPOAEs (**Fig. 2C**).

To further explore the cellular basis of this rapid progression, we performed immunofluorescence analysis of MYO7A and hair cell morphology at 8 weeks. By this stage, MYO7A expression was nearly absent throughout the cochlea in *ΔEnhancerA* mice (**Fig. 2D**), and was accompanied by extensive degeneration of hair cells in the basal turn, with partial loss observed in the middle turn. These results suggest that *EnhancerA* is not only essential for the early developmental expression of *Myo7a*, but also becomes increasingly critical for maintaining *Myo7a* expression and hair cell survival as the cochlea matures—potentially due to dynamic changes in chromatin accessibility during development.

Together, these findings demonstrate that *EnhancerA* plays a critical role in regulating MYO7A expression in a tonotopically graded manner. Its deletion disrupts hair bundle morphogenesis, compromises hair cell maintenance, and impairs long-term auditory function, initially affecting high-frequency regions and progressively extending toward lower-frequency areas with age

3.4. Deletion of *EnhancerA* causes reduced resting open probability of MET channels in tonotopically graded manner

Our previous work demonstrated that isoform-specific deletion of *Myo7a-C* results in approximately 80% reduction of MYO7A protein in IHCs, leading to decreased resting open probability and delayed activation kinetics of MET currents[6]. These findings established a role for MYO7A-C in maintaining resting tension on the MET complex in IHCs. However, the contribution of MYO7A to MET function in OHCs was not characterized in our previous study. The *ΔEnhancerA* mouse model presents an opportunity to address this gap. Unlike the isoform-specific KO, *ΔEnhancerA* mice exhibit reduced expression of all known *Myo7a* isoforms in both IHCs and OHCs. Furthermore, MYO7A loss occurs in a tonotopically graded manner, allowing us to correlate spatial differences in protein levels with MET channel properties, independent of isoform bias.

To assess MET function, we recorded transduction currents from OHCs in the basal and apical cochlea of *ΔEnhancerA* homozygous mice at postnatal day 4-5 (P4-5), using fluid jet stimulation and high-speed imaging to monitor bundle deflections. To avoid confounds from disrupted bundles, we confirmed that the stereocilia showed WT-like development starting at mid-basal area (**Supplementary Fig. 1A**). All recordings were restricted to regions with intact stereocilia morphology from the mid-basal to apical sections of the cochlea.

Apical OHCs—where MYO7A expression is reduced by only 50%—exhibited no significant differences in resting open probability, peak current, or adaptation compared to heterozygous controls (**Fig. 3A, B, E, F**). However, in mid-basal OHCs, where MYO7A levels are strongly reduced but bundles are still intact, sinusoidal stimulation revealed a significant decrease in the resting open probability of MET channels, while peak current amplitudes remained unchanged (**Fig. 3C, D**). Similarly, step-like stimuli confirmed a reduction in resting open probability, with no detectable changes in current amplitude or adaptation kinetics (**Fig. 3E, G; Supplementary Fig. 2A**). Collectively, these results confirm our previous study that MYO7A levels are critical for maintaining resting tension on the MET apparatus[6] .

3.5. SIX2 is tonotopically expressed in the cochlea

While *EnhancerA* confers a tonotopically graded expression pattern on *Myo7a* expression, its deletion disrupts both *Myo7a-C* and *Myo7a-N* isoforms, indicating that additional mechanisms are involved in mediating isoform-specific regulation. To identify potential trans-regulatory factors, we queried the Unbind2021[17] and ReMap2022[18] ChIP-seq databases and discovered a prominent SIX2 binding site centrally located within *EnhancerA*[19,20] (**Fig. 4A,B**). SIX2 is a homeodomain transcription factor known for its roles in kidney[21–24], craniofacial skeleton[25] development. Although haploinsufficiency of SIX2 has been associated with mild high-frequency hearing loss in humans[26], its function in auditory and vestibular hair cells remains largely uncharacterized.

First, we investigated the expression pattern of SIX2 in the mouse cochlea. Previously, it has been reported that a widely used commercially available SIX2 antibody also interacts with SIX1[19]. To circumvent this, we utilized the *Six2::cre- cre-egfp* mouse line and visualized EGFP expression as a proxy for SIX2 activity. At P5, we observed strong SIX2 driven EGFP signal in OHCs and a subset of supporting cells within the greater epithelial ridge (GER), with comparatively weaker expression in IHCs (**Fig. 4C–E**). Notably, SIX2 expression displayed a tonotopic gradient—highest in the basal cochlear turn and tapering toward the apex—mirroring the distribution of *Myo7a-N* isoform expression. This parallel pattern suggests a potential regulatory role for SIX2 in modulating *Myo7a-N* expression in the cochlea.

To confirm endogenous SIX2 expression and define its subcellular localization, we generated a *Six2-HA* knock-in (KI) mouse line, tagging the C-terminus of the endogenous

gene with an HA epitope. The HA tag did not affect SIX2 function, since *Six2-HA* homozygous mice developed normally, while SIX2 KO mice are known to die perinatally[21] . Immunostaining of these cochleae revealed a similar tonotopic pattern of SIX2-HA signal as observed in *Six2::cre-egfp* mice, with strong nuclear expression in OHCs and GER cells in the basal region, decreasing toward the apex (**Fig. 4F–H**). Consistent with previous findings, SIX2-HA expression was low in IHCs, supporting the idea that SIX2 acts as an OHC-specific transcription factor within the hair cell population. The nuclear enrichment of the HA signal further suggests that SIX2 is transcriptionally active in these cells.

Taken together, these findings identify SIX2 as a tonotopically expressed transcription factor with potential isoform-specific regulatory functions in cochlear hair cells, particularly in controlling *Myo7a-N* expression in OHCs.

3.6. Loss of SIX2 disrupts hair cell development and MYO7A levels in a tonotopic manner

Based on the expression pattern of SIX2 in the cochlea—particularly in hair cells—we hypothesized that SIX2 may play a critical role in hair cell development. To test this, we generated conditional knockout mice by crossing *Atoh1::cre* mice with *Six2*$^{flox/flox}$ mice (*Atoh1::cre*$^{+/-}$; *Six2*$^{flox/flox}$ mice referred to as, *Atoh1-Six2-cKO*), as global deletion of SIX2 results in early postnatal lethality[21]. In these conditional mutants, SIX2 is specifically deleted in hair cells during early embryonic development (embryonic day 12.5).

At P0, *Atoh1-Six2-cKO* cochleae exhibited a marked loss of OHCs, with the basal turn showing an almost complete absence of OHCs and the middle turn showing moderate loss. In contrast, the number of IHCs remained largely unaffected across all cochlear regions (**Fig. 5A–C**). This tonotopic pattern of OHC loss mirrors the gradient of SIX2 expression observed in hair cells (**Fig. 4C–H**).

Beyond cell loss, OHCs in *Atoh1-Six2-cKO* mice displayed disrupted spatial organization. While control cochleae (*Atoh1::cre*$^{+/-}$; *Six2*$^{+/+}$) show the characteristic three rows of OHCs, this arrangement was lost in the middle and basal turns of mutant cochleae (**Fig. 5D**). OHCs also lost proper alignment along the z-axis, showing inconsistent depth and malformed cell bodies (**Fig. 5D**). Furthermore, surviving OHCs exhibited abnormal morphology and severely disorganized or absent stereocilia bundles (**Fig. 5E**). IHCs retained hair bundles but lost the typical V-shaped organization and staircase-like structure of stereocilia, despite low or undetectable expression of SIX2 in IHCs, suggesting either a low-level requirement for SIX2 or indirect effects from surrounding cell disruption.

We hypothesized that SIX2 promotes the expression of the *Myo7a-N* isoform through interaction with *EnhancerA*, contributing to MYO7A abundance in OHCs. To test this, we quantified pan-MYO7A immunoreactivity in IHCs and OHCs across different cochlear regions at P0 (**Fig. 5F, G**). In *Atoh1-Six2-cKO* mice, the remaining OHCs displayed a

graded reduction of MYO7A signal, with the greatest loss in the basal turn and a milder reduction apically (**Fig. 5F, G**). In contrast, IHCs—where SIX2 is minimally expressed—showed no significant reduction in MYO7A levels. This spatially graded MYO7A reduction correlates with the pattern of SIX2 expression, supporting a role for SIX2 in regulating MYO7A levels and promoting early hair cell differentiation and/or development, particularly in OHCs.

3.7. SIX2 maintains hair cell integrity and isoform-specific MYO7A expression in the mature cochlea.

To investigate the role of SIX2 in mature hair cells, we generated conditional KO mice by crossing *Myo15a::cre* with *Six2*$^{flox/flox}$ mice (*Myo15a::cre*$^{+/-}$; *Six2*$^{flox/flox}$ mice referred to as *Myo15a-Six2-cKO, Myo15a::cre*$^{+/-}$; *Six2*$^{+/+}$ mice used as control). Since *Myo15a::Cre* expression begins during the early postnatal period[27], this approach allows SIX2 deletion after initial hair cell differentiation and development.

At 8 weeks of age, *Myo15a-Six2-cKO* mice showed no apparent loss of hair cells (**Fig. 6A**). However, by 16 weeks, we observed progressive degeneration of OHCs, starting in the basal cochlea and extending apically (**Fig. 6B–C**), consistent with the tonotopic expression pattern of SIX2. This degeneration was accompanied by progressive hearing loss, with threshold shifts first emerging at mid-to-high frequencies by 8 weeks and expanding to all frequencies by 16 weeks (**Fig. 6D–E**). These findings suggest that SIX2 is required for the maintenance of hair cell integrity post-development, and its deletion leads to hair cell degeneration and hearing impairment.

Since no hair cell loss was detected at 8 weeks, we analyzed *Myo7a* isoform expression at postnatal day 20 (P20) using qPCR, reasoning that transcript changes at this stage likely reflect regulatory effects rather than cell loss. Notably, expression of total *Myo7a* and the *Myo7a-N* isoform was significantly reduced in SIX2-deficient mice, whereas the *Myo7a-C* isoform remained unchanged (**Fig. 6F**). These results suggest that SIX2 regulates *Myo7a* expression in an isoform-specific manner.

We further examined the expression of other hair cell-specific genes. Transcript levels of *Atp8b1* and *Tmc1* were reduced in *Myo15a-Six2-cKO* mice, while *Tmc2* levels remained unchanged (**Fig. 6G**). The lack of change in *Tmc2* may be due to its naturally low expression in mature hair cells, making further reductions undetectable by qPCR.

Together, these data reveal that SIX2 plays a crucial role in maintaining gene expression in mature hair cells, including the regulation of specific *Myo7a* isoforms, and that its loss compromises hair cell survival and auditory function.

4. Discussion

EnhancerA orchestrates tonotopic *Myo7a* expression in cochlear hair cells

Cochlear hair cells express two isoforms of *Myo7a*, *Myo7a-C* and *Myo7a-N*, with complementary tonotopic and cell type–specific expression[15]. While IHCs predominantly express *Myo7a-C*, OHCs co-express both isoforms in opposing spatial gradients. Furthermore, these two isoforms exhibit distinct ATPase activity, suggesting their roles in regulating MET properties. Thus, understanding how this expression diversity is regulated is expected to be important for decoding their distinct functional roles.

Here, we identify *EnhancerA*, a conserved intronic *cis*-regulatory element, as essential for maintaining robust *Myo7a* expression in both IHCs and OHCs. Deletion of *EnhancerA* during early postnatal development causes a progressive, tonotopically graded reduction in MYO7A transcript and protein level, culminating in near-complete loss by 8 weeks. This suggests that *EnhancerA* activity becomes increasingly critical as chromatin landscapes mature.

Importantly, *EnhancerA* deletion impacts both isoforms, indicating that it serves as a shared enhancer of isoform-selective promoters. The widely used canonical promoter upstream of *Myo7a-C* is highly active in IHCs but weak in OHCs[6,13,14], suggesting that *Myo7a-N* is driven by an alternative promoter. A previous study in zebrafish identified two regulatory 'blocks' upstream of the *Myo7a* gene that drive hair cell–specific expression of reporter genes[12]. Our recent findings suggest that one of these blocks corresponds to the first exon of a previously uncharacterized *Myo7a* isoform we named *Myo7a-N*[15], while the other is located just upstream, consistent with the location of a putative *Myo7a-N* promoter. In the future, it will be important to investigate how *EnhancerA* interacts with these isoform-specific promoters to regulate MYO7A expression in a cell type– and isoform-specific manner.

MYO7A tunes MET gating

It has been proposed that MYO7A acts as a motor protein that provides tension to the MET complex at UTLDs[28–30]. However, due to the disruption of hair bundle development in MYO7A depletion models, it has been challenging to isolate its specific role in MET function. Previously, we employed the *Myo7a-ΔC* model to examine the effects of severe MYO7A depletion specifically in IHCs[6]. In this model, reduction of MYO7A at UTLDs led to decreased resting P_o and slowed onset of MET currents, supporting the hypothesis that MYO7A contributes to tensioning the MET complex.

In the current study, the *ΔEnhancerA* model serves as a tool to test MYO7A function, as it reduces expression of all MYO7A isoforms in both IHCs and OHCs. Notably, the tonotopic gradient of MYO7A depletion in this model enables investigation of MET function across a range of MYO7A expression levels. At P4-5, MYO7A reduction is most severe in basal OHCs, where we observed a significant decrease in MET resting P_o, while peak current amplitude and adaptation kinetics remained unaffected. In contrast, apical OHCs, which exhibited only mild MYO7A depletion, showed no measurable changes in MET properties. Together, these results reinforce our previous findings that MYO7A depletion leads to a reduction in tip-link tension[6].

Notably, a recent study reported that MYO7A loss in mature hair cells (P20–P30) led to reduced bundle stiffness and diminished peak MET currents, without affecting resting Po[4]. The contrast with our findings at P4-5 may be due to developmental stage–specific functions of MYO7A. During early postnatal stages, MYO7A may play a more active role in generating tip-link tension and supporting MET complex assembly, whereas in mature cells, its function may shift toward structural stabilization. Collectively, these results underscore the dynamic, isoform- and stage-dependent contributions of MYO7A to hair cell MET that warrants further research to gain a more complete picture.

Isoform-specific regulatory mechanism that drive *Myo7a* expression

Using publicly available ChIP-seq datasets, we identified a SIX2 binding site within *EnhancerA*[19]. Our data demonstrate that the expression pattern of SIX2 closely correlate with that of *Myo7a-N*, and further show that SIX2 preferentially regulates *Myo7a-N* expression, but not MYO7A-C. Together, these findings identify SIX2 as an isoform-specific *trans*-regulatory factor for *Myo7a*.

We propose that *EnhancerA* functions as a shared scaffold for transcriptional activation in both IHCs and OHCs, with isoform specificity determined by the local presence or absence of trans-acting factors such as SIX2. In OHCs, particularly in basal regions where SIX2 expression is highest, SIX2 may cooperate with *EnhancerA* to drive *Myo7a-N* expression via a potential *Myo7a-N* promoter, thereby establishing an increase in *Myo7a-N* levels toward cochlea base. In contrast, in IHCs, which express little or no SIX2, *EnhancerA* activity may preferentially couple with the canonical promoter of *Myo7a-C* via other transcription factors. This combinatorial mechanism—where a broadly active enhancer integrates input from spatially restricted transcription factors—offers a compelling explanation for the observed isoform gradients.

SIX2 is critical for hair cell development and maintenance

SIX family transcription factors are known to be critical for cell proliferation and differentiation, and ultimately the proper development of tissue. SIX1 and SIX2 share high similarity in amino-acid sequence, structural domains and DNA-binding motif. Both have been implicated in auditory system development, with SIX1 being extensively characterized for its essential role in early inner ear development[31–35]. Although SIX2's role in the cochlea has been less defined, a recent human genetic studies associate SIX2 haploinsufficiency with mid-high frequency hearing loss[26].

In this study, we demonstrated that deletion of SIX2 during development disrupts hair cell development, leading to a reduced number of OHCs and underdevelopment of both IHC and OHCs. Moreover, the deletion of SIX2 after hair cell differentiation and initial development causes loss of OHCs, which potentially result from the reduction of hair cell specific proteins such us MYO7A and TMC1. These findings indicate that SIX2 regulates a broader transcriptional program essential for OHC function and long-term maintenance.

Future studies leveraging SIX2-HA knock-in mice—which offer high antibody specificity—will enable chromatin profiling to map genomic regions directly bound by SIX2. Additionally, transcriptomic analyses such as RNA-seq will be instrumental in defining the downstream targets of SIX2 and elucidating its broader regulatory roles in the auditory system.

SIX2 likely operates within a wider transcriptional network involving other regulators such as ATOH1[36], POU4F3[37], and GFI1[38]. While ATOH1 initiates hair cell differentiation, factors like SIX2 may refine subtype identity and enforce region-specific gene expression. Meanwhile, EYA1/2 are known transcription co-factors that interact with SIX2 for gene expression, and EYA2 showed tonotopic hair-cell specific expression[39]. Interactions among these transcription factors are likely essential for shaping MYO7A isoform diversity and for establishing the tonotopic architecture of cochlear hair cells.

Implications for isoform-specific gene therapy

Our findings have direct translational relevance. MYO7A's cell type–specific and tonotopically graded expression presents both a challenge and an opportunity for precision gene therapy. *EnhancerA* and SIX2-responsive elements could be leveraged to design synthetic promoters that enable targeted transgene expression in IHCs or OHCs, or even regionally along the cochlear axis. This spatial control is especially valuable for treating MYO7A-linked disorders such as Usher syndrome type 1B, where both isoform specificity and cochlear location matter for therapeutic efficacy.

In summary, this study identifies *EnhancerA* and SIX2 as key regulators of MYO7A isoform expression in the cochlea, linking transcriptional control to regional and cell type–specific functional specialization. These findings deepen our understanding of cochlear gene regulation and lay the groundwork for targeted, isoform-aware therapies for sensorineural hearing loss.

5. Figures

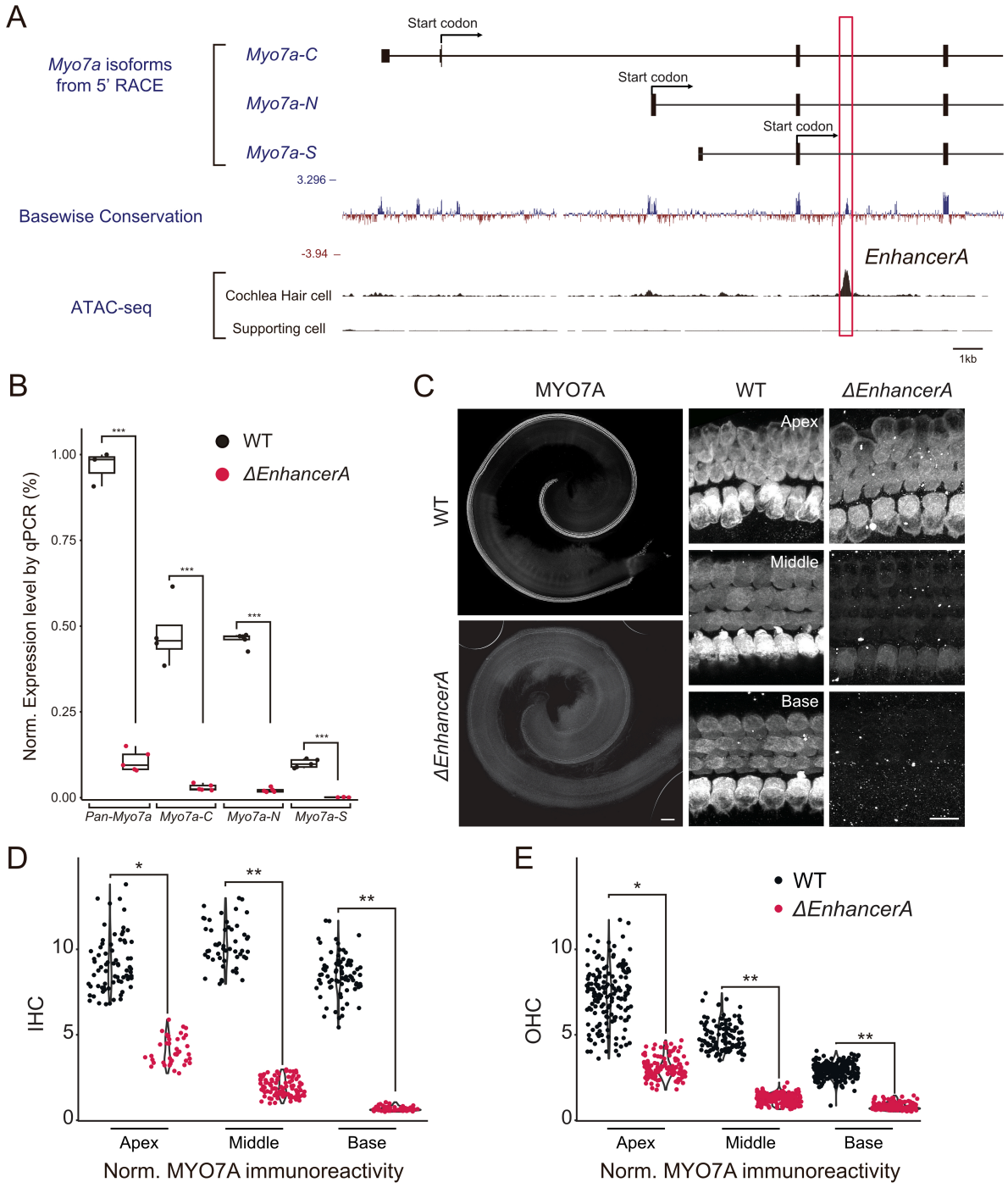

Figure 1: Enhancer A is required for tonotopically graded expression of *Myo7a*

A. Schematic indicating the transcriptional start sites of *Myo7a* isoforms. ATAC-seq tracks are derived from a publicly available dataset. *EnhancerA* is an around 400bp open chromatin region that locates in the third intron of *Myo7a-N*, which is indicated with red bracket (GRCm38/mm10: chr7: 98105422-98105821). This region is specifically knocked out in *ΔEnhancerA* mice without affecting exons. **B**. Normalized expression level of *Myo7a* isoforms measured by qPCR on P0 cochlear cDNA. *Myo7a* expression level is normalized to *Gapdh*. (WT vs. *ΔEnhancerA* mice t-test p-values of different isoforms: *pan-Myo7a*: 1.30e-4,

Myo7a-C=2.60e-3, *Myo7a-N*=1.32e-07, *Myo7a-S*=5.59e-05. Number of Cochlea: WT=8, *ΔEnhancerA*=8. Pipetting repetition=5 per group). Boxplots show medians, 25th, and 75th percentiles as box limits and minima and maxima as whiskers. **C**. Immunofluorescence images of whole mount *ΔEnhancerA* cochlea at P7. Compared to WT cochlea, *ΔEnhancerA* mice showed tonotopic reduction of MYO7A immunoreactivity, with a stronger reduction in the basal region and less reduction at the apical region. (Scale bar: left: 100 μm, right 10 μm). **D, E.** Quantification of MYO7A immunoreactivity in IHCs and OHC at P7. MYO7A signals were normalized to MYO6. (T-test on the average normalized MYO7A immunofluorescence signal of each cochlea. Number of cochlea: WT: 4; *ΔEnhancerA*: 4. T-test p-value between WT and *ΔEnhancerA*: IHC: base: 5.63e-3; middle: 1.10e-3; apex: 1.43e-2. OHC: base: 1.77e-3; middle: 8.17e-3; apex: 2.89e-2).

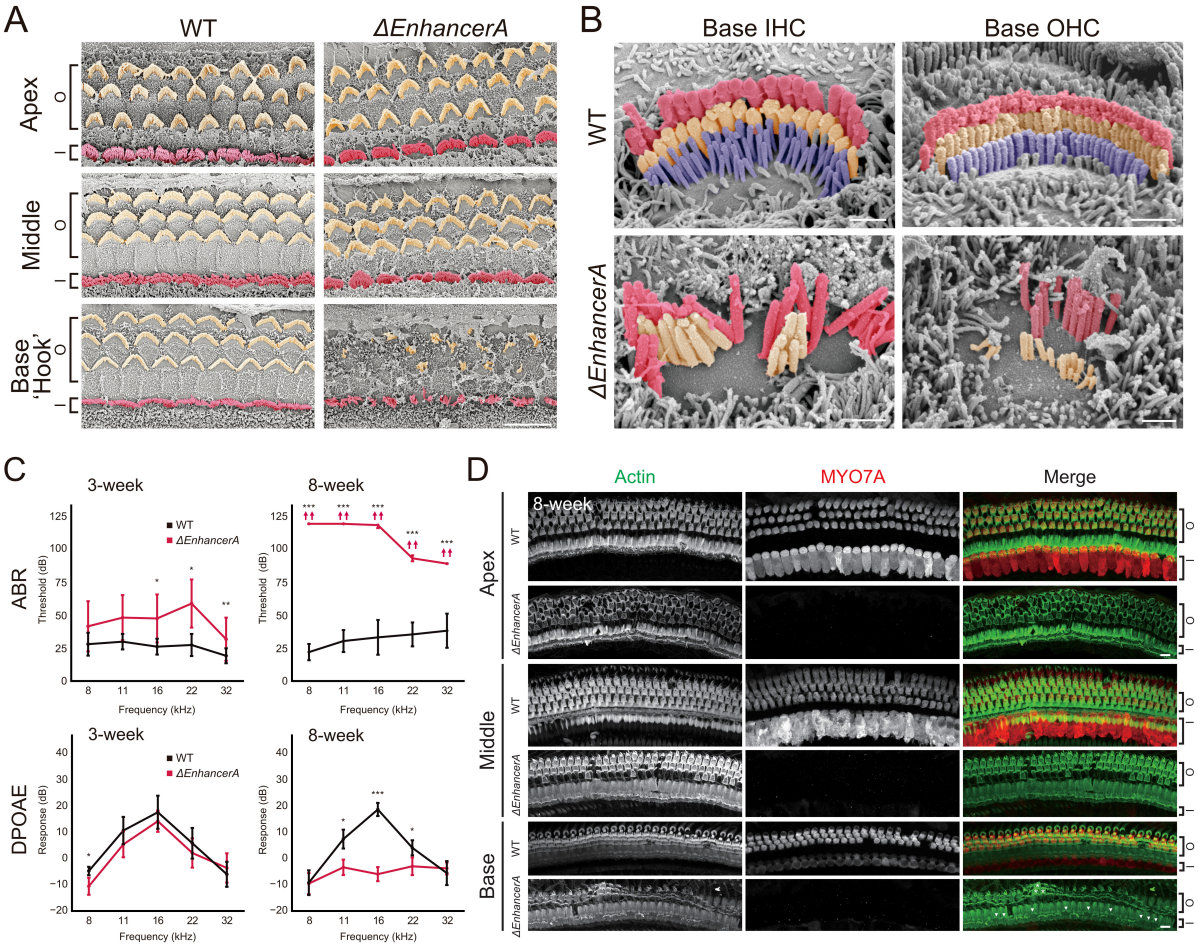

Figure 2: **Hair cell degeneration and hearing loss of *ΔEnhancerA* mice.**

A. Scanning electron microscopy (SEM) images of WT and *ΔEnhancerA* cochleae at P7. *ΔEnhancerA* hair cells display disorganized hair bundles near the base of the cochlea. (Scale bar: 10 μm). **B**. Higher-magnification SEM images of WT and *ΔEnhancerA* cochleae at P7 reveal detailed structural abnormalities in *ΔEnhancerA* hair bundles. (Scale bar: 1 μm). **C**. ABR thresholds and DPOAE respond of WT and *ΔEnhancerA* at 3 weeks and 8 weeks of age. *ΔEnhancerA* mice exhibit mild hearing loss at 3 weeks, which progresses to profound hearing loss by 8 weeks. (ABR ANOVA p-value: 3-week=1.25e-08, 8-week<2e-16. Number of animals: WT: 3-week=8, 8-week=9; *ΔEnhancerA*: 3-week=8, 8-week=5. DPOAE p-value: 3-week=0.0060, 8-week=1.12e-11. Number of animals: WT: 3-week=8, 8-week=10; *ΔEnhancerA*: 3-week=7, 8-week=5). Line-plots show means of the ABR or DPOAE response. Standard error is presented as error bars. **D**. Immunofluorescence images of WT and *ΔEnhancerA* mice at 8 weeks. MYO7A expression is nearly absent across all cochlear regions in *ΔEnhancerA* mice, accompanied by extensive hair cell loss. (Scale bar: 10 μm. Asterisk labels the remaining OHCs at basal regions of *ΔEnhancerA* mice. Arrow heads labels the IHCs loss).

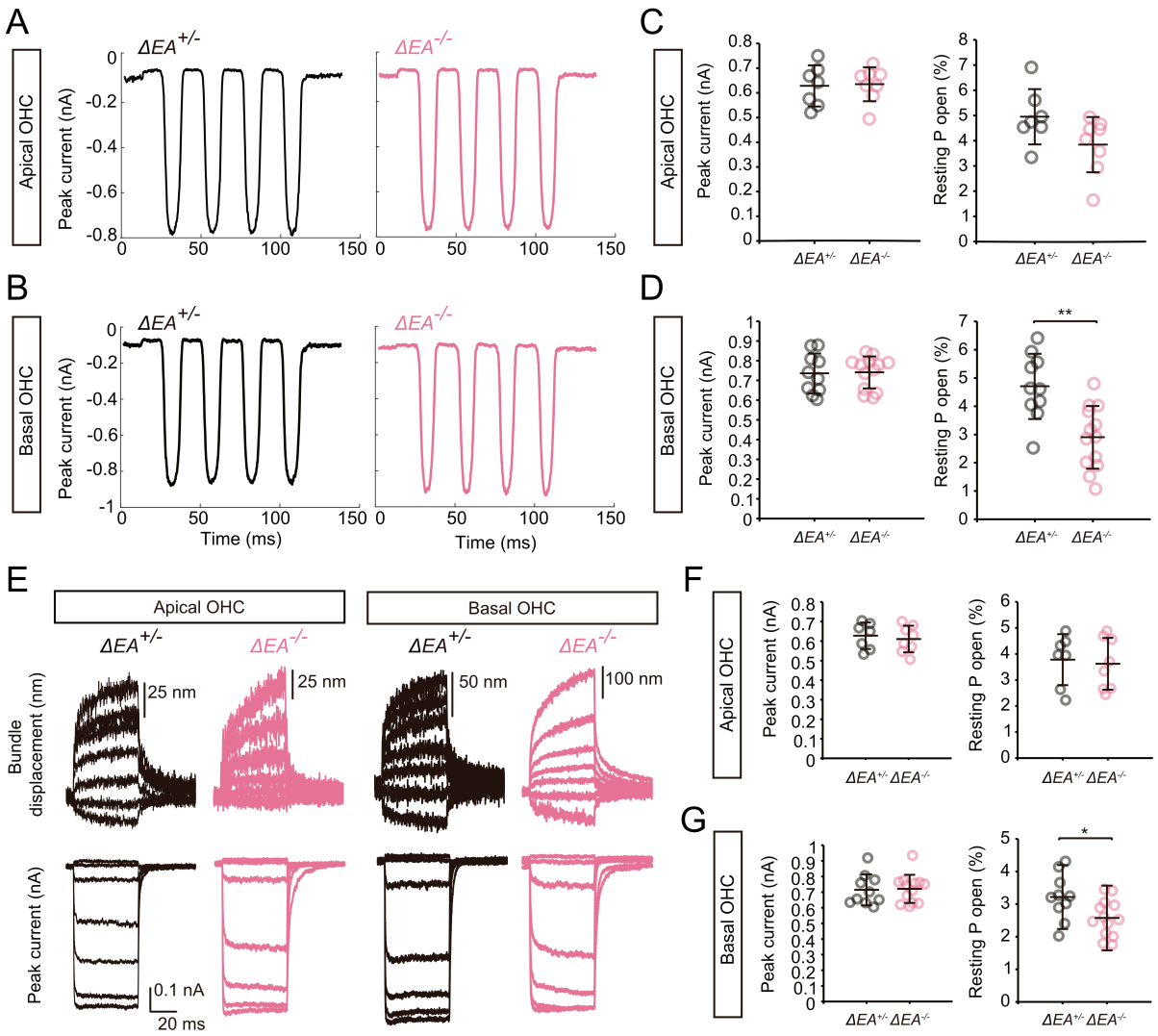

Figure 3: **Reduction of resting open probability of *ΔEnhancerA* OHC.**

A, **B**. Evaluation of MET current using sinusoidal signals. OHCs from the basal region of the cochlea were isolated at P4-P5. MET currents evoked by sine stimulation in heterozygous *ΔEnhancerA* ($\Delta EA^{+/-}$) OHC (black traces) and homozygous ($\Delta EA^{-/-}$) OHC (pink traces) are shown for the apical turn OHCs (top) and basal turn OHCs (bottom). **C, D**. Summary plots of the peak current and resting open probability (Resting P open) observed from MET currents in the apical turn (**C**) and basal turn (**D**). Resting open probability is estimated by dividing the resting current by the maximum MET current. Mean ± SD. ** $p \leq 0.01$. Number of cells (animals): Apical $\Delta EA^{+/-}$ 8 (8), Basal $\Delta EA^{+/-}$ 13 (13), Apical $\Delta EA^{-/-}$ 7 (7), Basal $\Delta EA^{-/-}$ 10 (10). **E**. Comparison of MET currents in apical and basal turns of $\Delta EA^{+/-}$ and $\Delta EA^{-/-}$ using step-like force stimuli. Displacement (top) and peak (bottom) current evoked by step-like force stimuli are shown. The intracellular solution contained 1 mM BAPTA, and a holding potential of -80 mV was used. Data are shown for the apical turn (left) and basal turn (right, shaded background). **F, G.** Summary plots of the peak current and resting open probability for apical (**F**) and basal (**G**) turn outer hair cells. Mean ± SD. * $p \leq 0.05$. Number of cells (animals): Apical $\Delta EA^{+/-}$ = 8 (8), Basal $\Delta EA^{+/-}$ = 13 (13), Apical $\Delta EA^{-/-}$ = 7 (7), Basal $\Delta EA^{-/-}$ = 10(10).

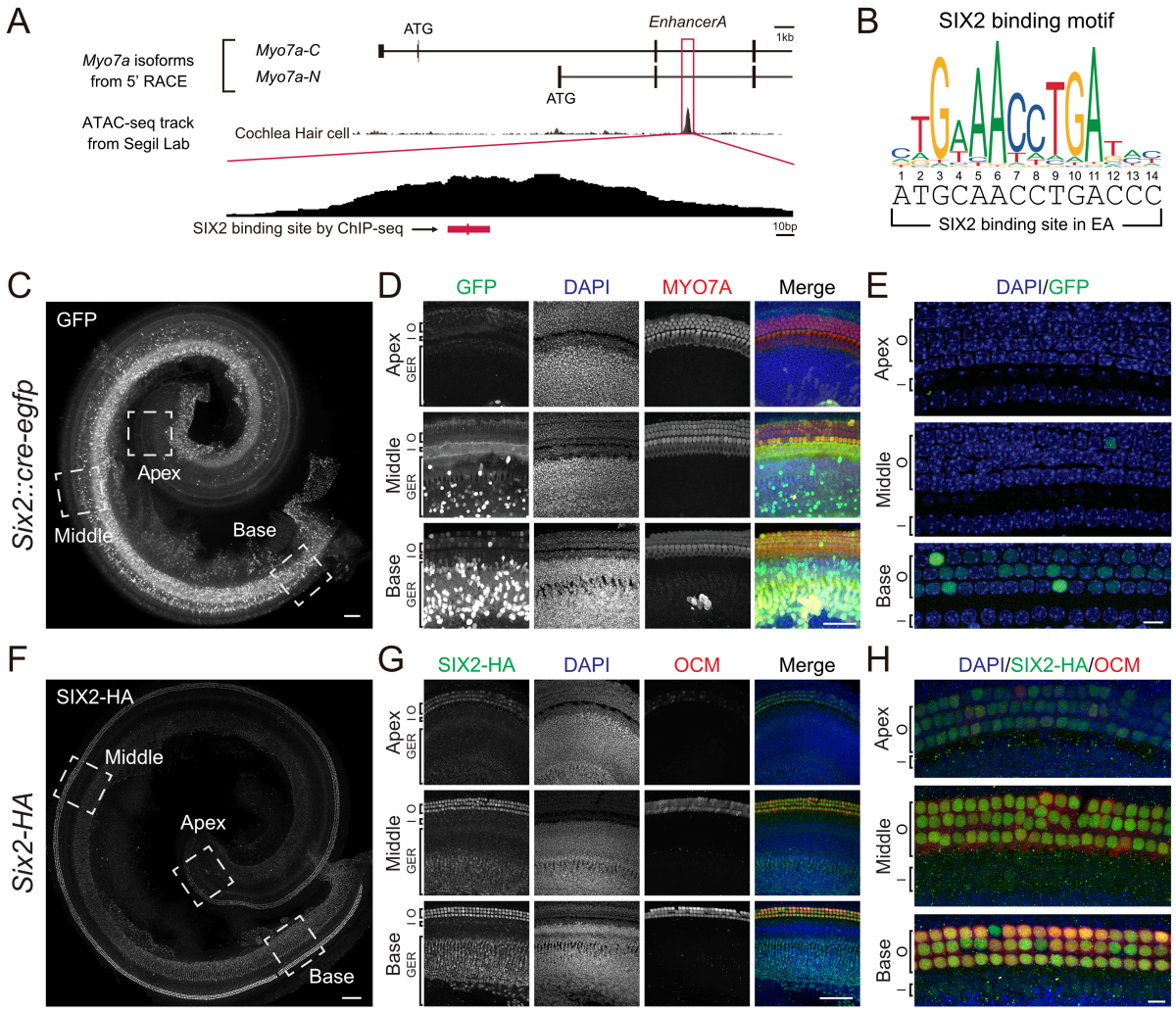

Figure 4: **Tonotopic expression of SIX2 in cochlea.**

A. The diagram demonstrating the SIX2 binding site in the *EnhancerA* tested by ChIP-seq. **B**. Human SIX2 binding motif reported by JASPAR database. The DNA sequence of SIX2 binding site in the *EnhancerA* is provided below the binding motif. **C**. Whole mount immunofluorescence image of *Six2::cre-egfp* cochlea at P5. GFP is tonotopically expressed in the cochlea, with a higher expression level at base and decrease toward apex. (Scale bar: 100 μm). **D**. immunofluorescence image of *Six2::cre-egfp* cochlea at base, middle and apex region. GFP is observed in the OHCs and GER cells. (Scale bar: 10 μm. "I": IHCs; "O": OHCs; "GER": greater epithelial ridge cells). **E**. immunofluorescence image of *Six2::cre-egfp* hair cell regions at base, middle and apex region. (Scale bar: 10 μm). **F**. Whole mount Immunofluorescence image of *Six2-HA* cochlea mice at P7. Similar with *Six2::cre-egfp* cochlea, SIX2 is also observed to be expressed tonotopically. (Scale bar: 100 μm). **G**. immunofluorescence image of *Six2-HA* cochlea at base, middle and apex region. HA-tag signal is observed in the OHCs and GER cells. Oncomodulin (OCM) is stained as OHC marker (Scale bar: 10 μm). **H**. immunofluorescence image of *Six2-HA* hair cell regions at base, middle and apex region. (Scale bar: 10 μm).

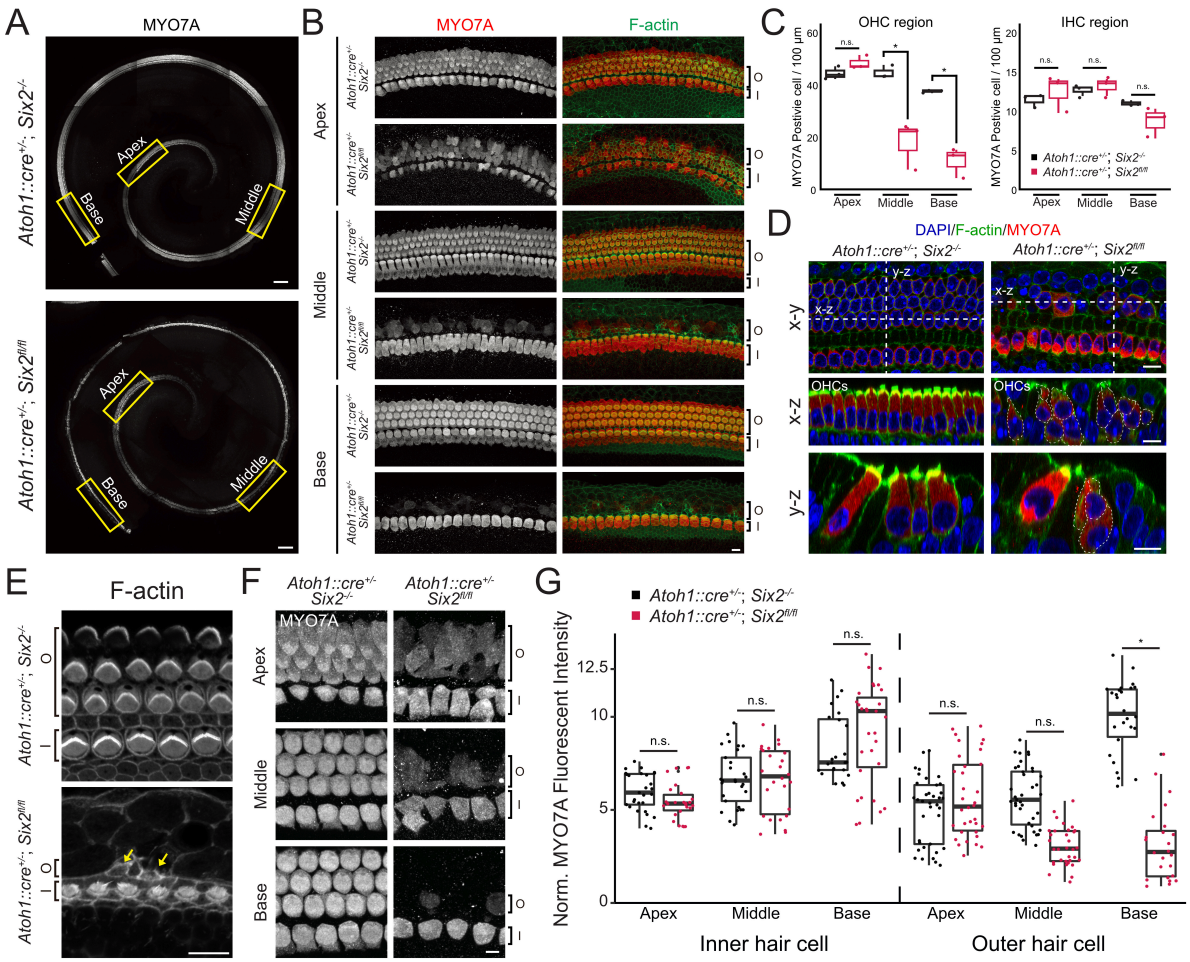

Figure 5: **SIX2 is necessary for hair cell development.**

A. Whole mount immunofluorescence image of control (*Atoh1::cre; Six2*$^{-/-}$) and *Six2* conditional deletion (*Atoh1::cre; Six2*$^{fl/fl}$) cochlea at P0. *Atho1::cre* induced conditional deletion of *Six2* result in tonotopic decrease of OHC. (Scale bar: 100 μm). **B**. Box-enlarged images of control and *Atoh1::cre; Six2*$^{fl/fl}$ cochlea. (Scale bar: 10 μm. "I": IHC; "O": OHC). **C**. Quantification of MYO7A positive cells in IHC and OHC. (T-test on the hair cell/100 μm of each cochlea. Number of cochlea: WT: 3; *ΔEnhancerA*: 3. T-test p-value between WT and *ΔEnhancerA*: IHC: base: 1.70e-1; middle: 5.18e-1; apex: 5.21e-1. OHC: base: 1.42e-2; middle: 2.77e-2; apex: 1.33e-1). **D**. Orthogonal view of control and *Atoh1::cre; Six2*$^{fl/fl}$ cochlea. The organization of OHCs is disrupted in the *Six2* conditional deletion cochlea in y and z axis. (Scale bar: 10 μm). **E**. Representative image of hair bundle of control and *Atoh1::cre; Six2*$^{fl/fl}$ cochlea. IHCs and OHCs has disorganized hair bundle. (Scale bar: 10 μm). **F**. Representative images of MYO7A signal at apical, middle and basal turn of cochlea. OHCs of *Atoh1::cre; Six2*$^{fl/fl}$ cochlea shows tonotopic reduction of MYO7A signal. (Scale bar: 10 μm). **G**. Quantification of MYO7A level in IHCs and OHCs at apical, middle and basal turn of cochlea. (T-test on the average normalized MYO7A immunofluorescence signal to backgroud of each cochlea. Number of cochlea: WT: 3; *ΔEnhancerA*: 3. T-test p-value between WT and *ΔEnhancerA*: IHC: base: 9.39e-1; middle: 8.98e-1; apex: 0.34e-1. OHC: base: 3.80e-2; middle: 1.25e-1; apex: 7.40e-1).

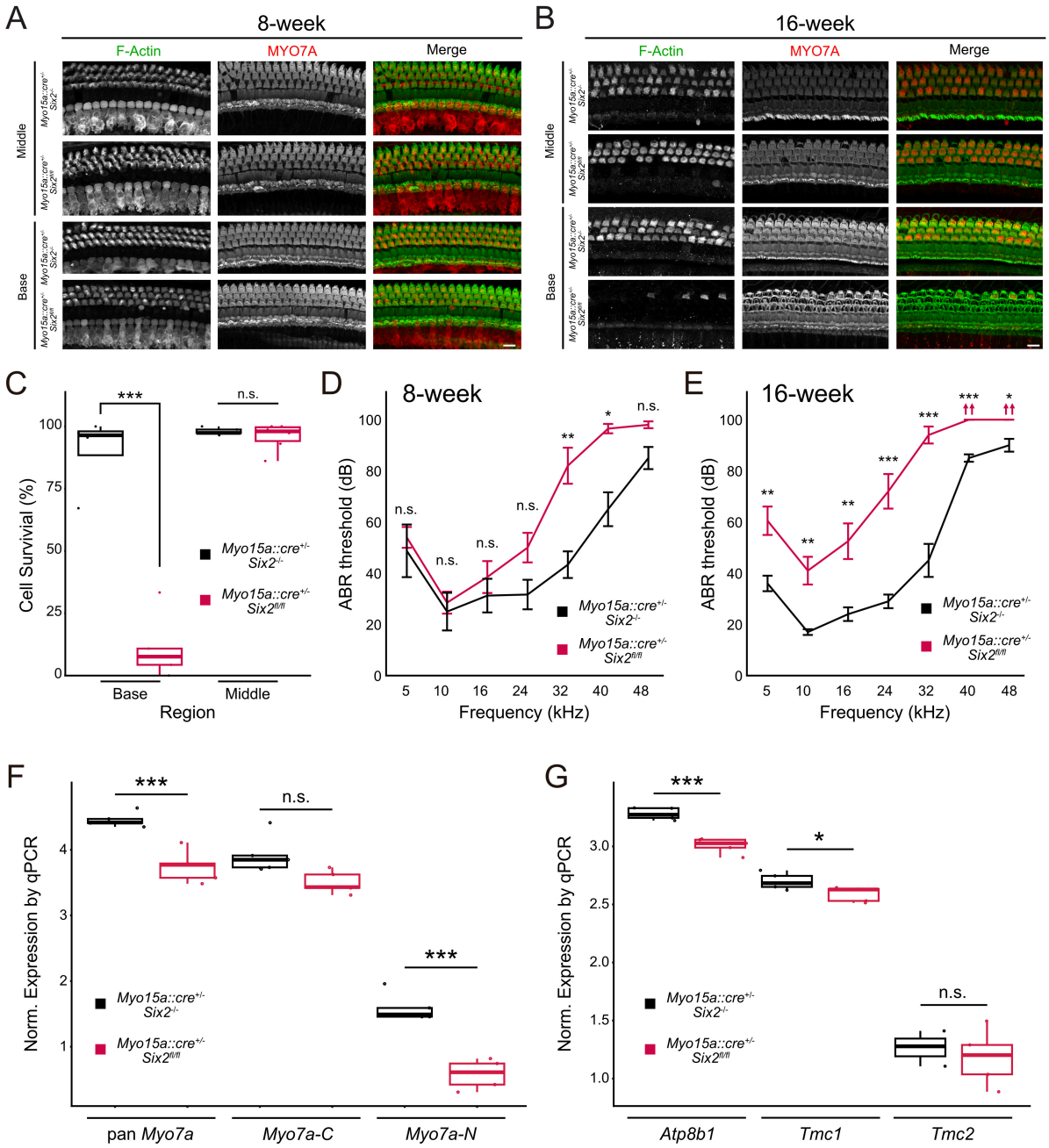

Figure 6: SIX2 is necessary for hair cell maintenance and MYO7A expression.

A. Representative image of 8-week control (*Myo15a::cre; Six2*$^{-/-}$) and *Myo15a::cre; Six2*$^{fl/fl}$ cochlea at middle and basal turns. (Scale bar: 10 µm). **B**. Representative image of 16-week control and *Myo15a::cre; Six2*$^{fl/fl}$ cochlea at middle and basal turns. *Myo15a::cre* induced conditional deletion of *Six2* result in OHC degeneration starting from basal turn. (Scale bar: 10 µm). **C**. Quantification of OHCs of control and *Myo15a::cre; Six2*$^{fl/fl}$ cochlea at middle and basal turns. (T-test p-value: base= 1.85e-4; middle= 3.93e-1. Number of animal: control: 3, *Myo15a::cre; Six2*$^{fl/fl}$ = 3). **D**. ABR test of control and *Myo15a::cre; Six2*$^{fl/fl}$ mice at 8 weeks. Mild ABR threshold shift is observed in the high frequencies tested. (ANOVA p-value: 3.23e-06. Number of animals: control = 4, *Myo15a::cre; Six2*$^{fl/fl}$ = 10). **E**. ABR test of control and *Myo15a::cre; Six2*$^{fl/fl}$ mice at 16 weeks. ABR threshold shift is observed in all of frequencies tested. (ANOVA p-value: 7.85e-15. Number of animals: control = 6, *Myo15a::cre; Six2*$^{fl/fl}$ =

10). **F**. Normalized expression level of *Myo7a* isoforms of 16-week control and *Myo15a::cre; Six2*$^{fl/fl}$ cochlear cDNA. *Myo7a* expression level is normalized to *Gapdh*. (T-test p-value: *pan-Myo7a* = 1.95e-4; *Myo7a-C* = 7.04e-2; *Myo7a-N* = 2.66e-3. Number of animal: control: 9, *Myo15a::cre; Six2*$^{fl/fl}$ = 7. Pipetting replication: 5 per group). **G**. Normalized expression level of selected hair cell specific genes of 16-week control and *Myo15a::cre; Six2*$^{fl/fl}$ cochlear cDNA. *Myo7a* expression level is normalized to *Gapdh*. (T-test p-value: *Atp8b1* = 7.68e-05; *Tmc1* = 3.09e-2; *Tmc2* = 6.08e-1. Number of animal: control: 9, *Myo15a::cre; Six2*$^{fl/fl}$ = 7. Pipetting replication: 5 per group).

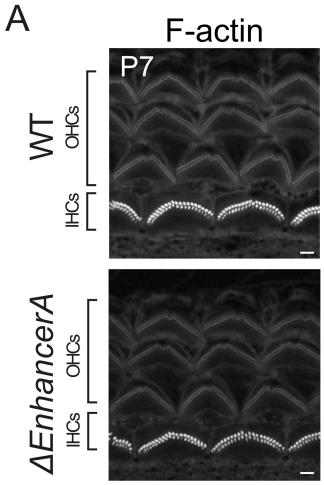

Supplementary Figure 1: A. *ΔEnhancerA* mice showed WT-like hair bundle at mid-basal turn of cochlea at P5.

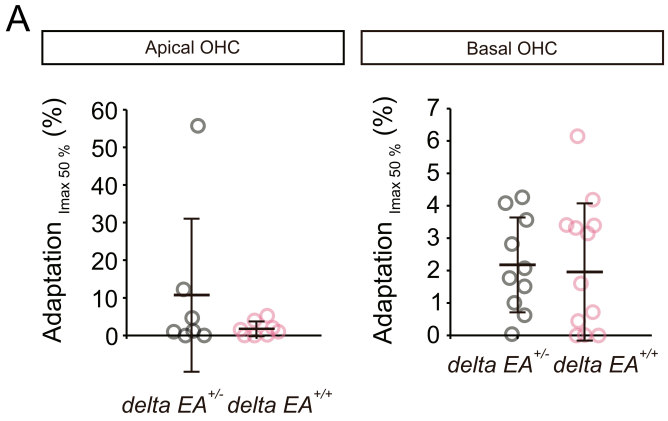

Supplementary Figure 2: A. Summary plots of the and adaptation for apical and basal turn OHCs. Mean ± SD. Number of cells (animals): Apical $\Delta EA^{+/-}$ = 8 (8), Basal $\Delta EA^{+/-}$ 13 (13), Apical $\Delta EA^{-/-}$ 7 (7), Basal $\Delta EA^{-/-}$ 10(10).

7. Methods:

Animal care and handling

The care and use of animals for all experiments described conformed to NIH guidelines. Experimental mice were housed in a 12:12 hour light:dark cycle with free access to chow and water in standard laboratory cages in a temperature and humidity-controlled vivarium. The protocols for the care and use of animals were approved by the Institutional Animal Care and Use Committees at the University of Virginia, the University of Colorado Denver, and the National Institute on Deafness and Other Communication Disorders. All the institutions mentioned above are accredited by the American Association for the Accreditation of Laboratory Animal Care. C57BL/6J (Bl6, from Jackson Laboratory, ME, USA) mice and sibling mice served as control mice for this study. Neonatal mouse pups (P0–P5) were sacrificed by rapid decapitation. Mature mice were euthanized by CO_2 asphyxiation followed by cervical dislocation.

Generation of Mouse strains for this study

For CRISPR/Cas mediated generation of the mouse models, we used the online tool CRISPR (http://crispor.tefor.net/crispor.py) to select suitable target sequences to ablate *Myo7a* isoforms. Single-guide (sg)RNAs are purchased from IDT (Integrated DNA Technologies, IA, USA). To produce genetically engineered mice, fertilized eggs were coinjected with Cas9 protein (PNA Bio, 50 ng/μl) and the sgRNA (30 ng/μl). Two-cell stage embryos were implanted on the following day into the oviducts of pseudopregnant ICR female mice (Envigo). Genotyping was performed by PCR amplification of the region of interest. Target sequences, sgRNAs, repair templates, and genotyping primers are listed below:

***ΔEnhancerA* mice:**

To ensure the large deletion of *EnhancerA*, a pair of guide RNA surrounding the *EnhancerA* are injected.

sgRNA1: 5'-ACAACAGCGACUUCCCUGCAUGG-3', sgRNA2: 5'-CCTACGTTCCTAGCCAGTCTCGC-3'. Genotyping primers: Forward: 5'-ACCATGACCCCATAAGGTTC-3', WT reverse: 5'-GGGATGAATCATCACTCCTGC-3', Mutant Reverse: 5'-AGTGTTCTCCCGAGAGCCTTTC-3'.

***Six2-HA* mouse:**

sgRNA: 5'-AGAGCTCTGTTCGCCTCCGG-3'. Repair template: GCGGCGCGGACCCACTGCAGCATCACCACAGCCTGCAGGACTCCATACTCAACCCCATGTCGGCCAACCTTGTGGACCTGGGCTCCTACCCATACGATGTTCCAGATTACGCTTAGAGCTCTGTTCGCCTCCGGGCGCTTGCTTTCCGTGCTTGATGAAGCGGTGTGGGAGGGCGATAGATTCTGGAGTCTGTGCCGCGT. Genotyping primers: Forward: 5'-TCCATACTCAACCCCATGTCGG-3', Reverse: 5'-CCAAAGGATACCGAGCAGACCA-3'.

***Myo15a-Cre*:**

To generate a *Myo15a-Cre* knockin (KI) mouse line, CRISPR/Cas9-mediated genome engineering was used to insert a "Cre-rBG (rat beta-globin intron) polyA" cassette upstream of the translational start codon (ATG) in exon 2 of the mouse *Myo15* gene (NCBI Reference Sequence: NM_010862.2), which is located on chromosome 11 and contains 66 exons (Ensembl Transcript: ENSMUST00000071880). The cassette was placed under the control of the endogenous *Myo15a* promoter to ensure physiologically

relevant Cre expression. Homology arms (~2–3 kb) flanking the insertion site were amplified by high-fidelity PCR using BAC clone RP23-329M3 as a template and assembled with the Cre-rBG cassette into the targeting vector. For genome editing, Cas9 protein, guide RNAs (gRNAs), and the targeting vector were co-injected into fertilized C57BL/6J one-cell embryos. Two gRNAs were designed to flank the insertion site with minimal predicted off-target activity: gRNA-A1 (GAGGGCCACCATGGCGGATG) matching the forward strand and gRNA-B1 (TTTCTTCTCCTCATCCGCCA) matching the reverse strand. Injected embryos were transferred into pseudopregnant females, and resulting pups were genotyped by PCR using genomic DNA from tail biopsies. Correct integration of the cassette was confirmed by Sanger sequencing across the homology arm–cassette junctions. The mouse line was generated by Cyagen Biosciences (Santa Clara, CA), and correctly targeted founders were bred with C57BL/6J animals to establish a stable *Myo15a-Cre* line.

Six2::cre-egfp mice is purchased from The Jackson Laboratory (Strain #:009606), and *Six2*$^{flox/flox}$ are generated by previous studies from other labs. The genotyping methods are provided by their corresponding reference[40,42].

Quantitative polymerase chain reaction (qPCR)

qPCR primers were designed to detect either *pan-Myo7a* transcripts or *Myo7a* isoform-specific transcripts to evaluate their expression levels. Total RNA was extracted using TRIzol reagent (15596026, ThermoFisher Scientific). Reverse transcription was performed using the SuperScript™ IV Reverse Transcription system (18090010, ThermoFisher Scientific). qPCR reactions were conducted using iTaq Universal SYBR Green Supermix (1725121, Bio-Rad, CA, USA) on a CFX Opus 384 Real-Time PCR System (12011319, Bio-Rad) for fluorescence measurement. Following analysis and plotting is done by R (version 4.4.1).

Primers: *pan-Myo7a*: forward: 5'-CCTTCTCATTCGCTACCGGG-3', reverse: 5'-*Myo7a-C*: forward: 5'-CCGGTTGTTGCGTTTCATGT-3', reverse: 5'-CCGACTCCCCGCTGATAATAC-3' ; *Myo7a-N*: forward: 5'-GTGCGAAACTTGAACCAAACG-3', reverse: 5'-CCGACTCCCCGCTGATAATAC-3' ; *Myo7a-S*: forward: 5'-ACAACAGCGACUUCCCUGCAUGG-3', reverse: 5'-CCGACTCCCCGCTGATAATAC-3' ; *Atp8b1*: forward: 5'-ACGGCCGGTGGTCTTACATA-3', reverse: 5'-GCTTGTCACTCACGTCCTGAT-3' ; *Tmc1*: forward: 5'-GTGGGCCCTTCAGTGGTAAA-3', reverse: 5'-TTTCTGGCCCTTGGCAGTAG-3' ; *Tmc2*: forward: 5'-GCCGGAAGGATCCTGCTAAG-3', reverse: 5'-CAAGGAAGTGGACCTGGGTT-3'.

Immunofluorescence

Inner ear organs were fixed in 3% paraformaldehyde (PFA, Electron Microscopy Sciences, PA) immediately after dissection for 20 min. Samples were washed three times with phosphate-buffered saline (GIBCO® PBS, Thermo Fisher Scientific, Waltham, MA) for 5 min each. After blocking for 2 h with blocking buffer (1% bovine serum albumin, 3% normal donkey serum, and 0.2% saponin in PBS), tissues were incubated in blocking buffer containing primary antibody at 4 °C overnight. The following antibodies were used in this study: rabbit polyclonal Myosin-VIIa antibody (catalog#: 25-6790, Proteus Biosciences Inc, Ramona, CA. 1:100), mouse monoclonal Myosin-VI antibody

(A-9, Santa Cruz, 1:100), rabbit anti-HA antibody (C29F4, Cell Signaling Technologies, Danvers, MA). Fluorescence imaging was performed using a Leica Stellaris 5 Confocal Microscope Platform or Zeiss LSM880 with AiryScan.

Hearing tests in mice

Mice were anesthetized with a single intraperitoneal injection of 100 mg/kg ketamine hydrochloride (Fort Dodge Animal Health) and 10 mg/kg xylazine hydrochloride (Lloyd Laboratories). ABR and DPOAE were performed in a sound-attenuating cubicle (Med-Associates, product number: ENV-022MD-WF), and mice were kept on a Deltaphase isothermal heating pad (Braintree Scientific) to maintain body temperature.

ABRs of *ΔEnhancerA* mice their BL6 controls were conducted on the equipment purchased from Intelligent Hearing Systems (Miami, Fl). Recordings were captured by subdermal needle electrodes (FE-7; Grass Technologies). The non-inverting electrode was placed at the vertex of the midline, the inverting electrode over the mastoid of the right ear, and the ground electrode on the upper thigh. Stimulus tones (pure tones) were presented at a rate of 21.1/s through a high-frequency transducer (Intelligent Hearing Systems). Responses were filtered at 300–3000 Hz, and threshold levels were determined from 1024 stimulus presentations at 8, 11.3, 16, 22.4, and 32 kHz. Stimulus intensity was decreased in 5–10 dB steps until a response waveform could no longer be identified. Stimulus intensity was then increased in 5 dB steps until a waveform could again be identified. If a waveform could not be identified at the maximum output of the transducer, a value of 5 dB was added to the maximum output as the threshold.

DPOAEs of the same group of WT and *Myo7a-ΔC* mice were recorded. While under anesthesia for ABR testing, DPOAE was recorded using SmartOAE ver. 5.20 (Intelligent Hearing Systems). A range of pure tones from 8 to 32 kHz (16 sweeps) was used to obtain the DPOAE for the right ear. DPOAE recordings were made for *f*2 frequencies from 8.8 to 35.3 kHz using a paradigm set as follows: $L1 = 65$ dB, $L2 = 55$ dB SPL, and $f_2/f_1 = 1.22$.

ABRs of *Myo15a::cre; Six2*$^{fl/fl}$ mice and its corresponding control are conducted on RZ6 Multi-I/O Processor (Tucker Davis, FL 32615 USA) with Medusa4Z ABR Amplifier. Responses are averaged by 512 stimulus sweeps presentations at 5, 10, 16, 24, 32, 40 and 48 kHz. Same ABR threshold determination strategies mentioned above are applied.

Whole-cell voltage-clamp electrophysiology recordings

Electrophysiological recordings

Whole-cell patch clamp experiments were conducted on the first or second row of outer hair cells or type II extrastriolar vestibular hair cells using an Axon 200B amplifier or a Multiclamp 700B (Molecular Devices). Initially, a patch pipette filled with extracellular solution was used to clean the epithelium, and 2-3 adjacent cells near the target cell were removed. Subsequently, a patch pipette filled with intracellular solution was used to perform the whole-cell patch clamp on the cell. Apical perfusion was continuously maintained until a gigaseal was performed. After breakthrough of the patch membrane to enter whole cell configuration, a minimum waiting time of 5 minutes was allowed for the intracellular solution to equilibrate. A fluid jet, using thin-walled borosilicate pipettes (World Precision Instrument), was then applied to deliver step-like force stimuli to the hair bundle. Experiments were performed at 18-22°C. Whole-cell currents were filtered at 10 kHz and sampled at 50 kHz using USB-

6356 or USB6366 (National Instruments) controlled by jClamp (SciSoft Company). All experiments used -80 mV holding potential unless otherwise noted and did not account for the liquid junction potential. In the LDM experiment, the MET current was first measured at -80 mV using step-like force stimuli, followed by LDM at +80 mV for approximately 10 seconds. After LDM, mechanotransduction current was measured again at -80 mV with step-like force stimuli. We adopted the results measured at -80 mV after LDM as noted. Iontophoesis experiments were done with pipette resistances in the range 5-7 MΩ. Iontophoresis retention current was 10 nA and ejection currents of 700-1000 nA was applied in increments of 1 second until peak MET current was near 100 pA.

Hair-bundle stimulation and motion recording

For most of the electrophysiological recordings, hair bundles were stimulated with a custom three-dimensional—printed fluid jet driven by a piezoelectric disc bender (27 mm, 4.6 kHz; Murata Electronics or PUI Audio). Thin-wall borosilicate pipettes were pulled to tip diameters of 5 to 15 µm, filled with extracellular solution, and mounted in the fluid-jet stimulator. The piezoelectric disc bender was driven by waveforms generated using jClamp. Stimulus waveforms were filtered using an eight-pole Bessel filter at 1 kHz (L8L 90PF, Frequency Devices Inc.) and variably attenuated (PA5, Tucker Davis) before being sent to a high-voltage/high-current Crawford amplifier to drive the piezoelectric disc bender. During stimulations, videos were taken of the hair-bundle motion with high-speed imaging at 10,000 frames per second using a Phantom Miro 320s or Veo 410L camera (Vision Research) when illuminated with a TLED+ with an LED centered at 530 nm (Sutter Instruments). Videos were saved for each stimulation and analyzed offline. Hair bundle displacement was determined as described previously[41,43,44]. Briefly, hair bundle position was extracted using a Gaussian fit to a high-pass–filtered hair-bundle image for a given vertical row of pixels in the image.320s or Veo 410L camera (Vision Research) when illuminated with a TLED+ with an LED centered at 530 nm (Sutter Instruments). Videos were saved for each stimulation and analyzed offline. Hair bundle displacement was determined as described previously12,33,58. Briefly, hair bundle position was extracted using a Gaussian fit to a high-pass–filtered hair-bundle image for a given vertical row of pixels in the image.

Scanning electron microscopy

Adult mice were euthanized by CO2 asphyxiation before intracardiac perfusion with 2.5% glutaraldehyde (Electron Microscopy Sciences, Hatfield, PA) and 2% PFA. The otic capsule was dissected and incubated in postfixation buffer at 4 °C overnight (2.5% glutaraldehyde, in 0.1 M cacodylate buffer, with 3 mM CaCl2). For neonatal mouse pups, the samples were dissected and treated with postfixation buffer immediately. The otic capsules from adult mice were incubated for two weeks in 4.13% EDTA for decalcification and then further dissected to expose the organ of Corti. Samples underwent the OTOTO procedure and were dehydrated using gradient ethanol and critical point drying. After sputter coating with platinum, the samples were imaged on Zeiss Sigma VP HD field emission SEM using the in-lens secondary electron detector.

6. Reference:

1. Hasson, T., Heintzelman, M.B., Santos-Sacchi, J., Corey, D.P., and Mooseker, M.S. (1995). Expression in cochlea and retina of myosin VIIa, the gene product defective in Usher syndrome type IB. Proc. Natl. Acad. Sci. U. S. A. *92*, 9815–9819. https://doi.org/10.1073/pnas.92.21.9815.

2. Well, D., Blanchard, S., Kaplan, J., Guilford, P., Gibson, F., Walsh, J., Mburu, P., Varela, A., Levilliers, J., Weston, M.D., et al. (1995). Defective myosin VIIA gene responsible for Usher syndrome type IB. Nature *374*, 60–61. https://doi.org/10.1038/374060a0.

3. Self, T., Mahony, M., Fleming, J., Walsh, J., Brown, S.D., and Steel, K.P. (1998). Shaker-1 mutations reveal roles for myosin VIIA in both development and function of cochlear hair cells. Development *125*, 557–566.

4. Anna Underhill, Samuel Webb, Fiorella C Grandi, Jing-Yi Jeng, Jacques B de Monvel, Baptiste Plion, Adam J Carlton, Ana E Amariutei, Niovi Voulgari, Francesca De Faveri, Federico Ceriani, Mirna Mustapha, Stuart L Johnson, Saaid Safieddine, Corné J Kros, W.M. (2025). MYO7A is required for the functional integrity of the mechanoelectrical transduction complex in hair cells of the adult cochlea. Proc. Natl. Acad. Sci. *120*. https://doi.org/10.1073/pnas.2414707122.

5. Corns, L.F., Johnson, S.L., Roberts, T., Ranatunga, K.M., Hendry, A., Ceriani, F., Safieddine, S., Steel, K.P., Forge, A., Petit, C., et al. (2018). Mechanotransduction is required for establishing and maintaining mature inner hair cells and regulating efferent innervation. Nat. Commun. 2018 91 *9*, 1–15. https://doi.org/10.1038/s41467-018-06307-w.

6. Li, S., Mecca, A., Kim, J., Caprara, G.A., Wagner, E.L., Du, T., Petrov, L., Xu, W., Cui, R., Rebustini, I.T., et al. (2020). Myosin-VIIa is expressed in multiple isoforms and essential for tensioning the hair cell mechanotransduction complex. Nat. Commun., 1–15. https://doi.org/10.1038/s41467-020-15936-z.

7. Well, D., Blanchard, S., Kaplan, J., Guilford, P., Gibson, F., Walsh, J., Mburu, P., Varela, A., Levilliers, J., Weston, M.D., et al. (1995). Defective myosin VIIA gene responsible for Usher syndrome type IB. Nat. 1995 3746517 *374*, 60–61. https://doi.org/10.1038/374060a0.

8. Weil, D., Lévy, G., Sahly, I., Lévi-Acobas, F., Blanchard, S., El-Amraoui, A., Crozet, F., Philippe, H., Abitbol, M., and Petit, C. (1996). Human myosin VIIA responsible for the Usher 1B syndrome: A predicted membrane-associated motor protein expressed in developing sensory epithelia. Proc. Natl. Acad. Sci. U. S. A. *93*, 3232–3237. https://doi.org/10.1073/pnas.93.8.3232.

9. Liu, X., Walsh, J., Mburu, P., Kendrick-jones, J., Cope, M.J.T. V, Steel, K.P., and Brown, S.D.M. (1997). Mutations in the myosin VIIA gene cause non-syndromic recessive deafness. 188–190. https://doi.org/10.1038/ng0697-188.

10. Liu, X.-Z., Walsh, J., Tamagawa, Y., Kitamura, K., Nishizawa, M., Steel, K.P., and Brown, S.D.M. (1997). Autosomal dominant non-syndromic deafness caused by a mutation in the myosin VIIA gene. Nat. Genet. *17*, 268–269. https://doi.org/10.1038/ng1197-268.

757 11. Boëda, B., Weil, D., and Petit, C. (2001). A specific promoter of the sensory cells of the inner
758 ear defined by transgenesis. Hum. Mol. Genet. *10*, 1581–1589.
759 https://doi.org/10.1093/hmg/10.15.1581.

760 12. Ernest, S., and Rosa, F.M. (2015). A genomic region encompassing a newly identified exon
761 provides enhancing activity sufficient for normal myo7aa expression in zebrafish sensory hair
762 cells. Dev. Neurobiol. *75*, 961–983. https://doi.org/10.1002/dneu.22263.

763 13. Kawashima, Y., Géléoc, G.S.G., Kurima, K., Labay, V., Lelli, A., Asai, Y., Makishima, T., Wu,
764 D.K., Santina, C.C. Della, Holt, J.R., et al. (2011). Mechanotransduction in mouse inner ear
765 hair cells requires transmembrane channel – like genes. J. Clin. Invest. *121*, 4796–4809.
766 https://doi.org/10.1172/JCI60405DS1.

767 14. Park, S., Jang, S., Lee, J.-H., Kim, S.-H., and Ryoo, Z.Y. (2017). Attempted rescue of circling
768 mice by hair cell-specific expression (Myo7a promoter) of tmie transgene. Med. Weter. *73*,
769 399–403. https://doi.org/10.21521/mw.5744.

770 15. Sihan Li, Jinho Park, Tobey M. Phan, Edward H. Egelman, Jonathan E. Bird, J.-B.S. (2025).
771 Tonotopic Specialization of MYO7A Isoforms in Auditory Hair Cells. bioRxiv *6*.
772 https://doi.org/https://doi.org/10.1101/2025.04.01.646665.

773 16. Jen, H.I., Hill, M.C., Tao, L., Sheng, K., Cao, W., Zhang, H., Yu, H. V., Llamas, J., Zong, C.,
774 Martin, J.F., et al. (2019). Transcriptomic and epigenetic regulation of hair cell regeneration in
775 the mouse utricle and its potentiation by Atoh1. Elife *8*, 1–27.
776 https://doi.org/10.7554/eLife.44328.

777 17. Puig, R.R., Boddie, P., Khan, A., Castro-Mondragon, J.A., and Mathelier, A. (2021). UniBind:
778 maps of high-confidence direct TF-DNA interactions across nine species. BMC Genomics *22*,
779 1–17. https://doi.org/10.1186/s12864-021-07760-6.

780 18. Hammal, F., De Langen, P., Bergon, A., Lopez, F., and Ballester, B. (2022). ReMap 2022: A
781 database of Human, Mouse, Drosophila and Arabidopsis regulatory regions from an integrative
782 analysis of DNA-binding sequencing experiments. Nucleic Acids Res. *50*, D316–D325.
783 https://doi.org/10.1093/nar/gkab996.

784 19. O'Brien, L.L., Guo, Q., Bahrami-Samani, E., Park, J.S., Hasso, S.M., Lee, Y.J., Fang, A., Kim,
785 A.D., Guo, J., Hong, T.M., et al. (2018). Transcriptional regulatory control of mammalian
786 nephron progenitors revealed by multi-factor cistromic analysis and genetic studies
787 https://doi.org/10.1371/journal.pgen.1007181.

788 20. Rauluseviciute, I., Riudavets-Puig, R., Blanc-Mathieu, R., Castro-Mondragon, J.A., Ferenc, K.,
789 Kumar, V., Lemma, R.B., Lucas, J., Chèneby, J., Baranasic, D., et al. (2024). JASPAR 2024:
790 20thãnniversary of the open-access database of transcription factor binding profiles. Nucleic
791 Acids Res. *52*, D174–D182. https://doi.org/10.1093/nar/gkad1059.

792 21. Self, M., Lagutin, O. V., Bowling, B., Hendrix, J., Cai, Y., Dressler, G.R., and Oliver, G. (2006).
793 Six2 is required for suppression of nephrogenesis and progenitor renewal in the developing
794 kidney. EMBO J. *25*, 5214–5228. https://doi.org/10.1038/sj.emboj.7601381.

795 22. Weber, S., Taylor, J.C., Winyard, P., Baker, K.F., Sullivan-Brown, J., Schild, R., Knüppel, T.,

796 Zurowska, A.M., Caldas-Alfonso, A., Litwin, M., et al. (2008). SIX2 and BMP4 mutations
797 associate with anomalous kidney development. J. Am. Soc. Nephrol. *19*, 891–903.
798 https://doi.org/10.1681/ASN.2006111282.

799 23. Li, J., Xu, J., Jiang, H., Zhang, T., Ramakrishnan, A., Shen, L., and Xu, P.X. (2021). Chromatin
800 remodelers interact with Eya1 and Six2 to target enhancers to control nephron progenitor cell
801 maintenance. J. Am. Soc. Nephrol. *32*, 2815–2833. https://doi.org/10.1681/ASN.2021040525.

802 24. Xu, J., Wong, E.Y.M., Cheng, C., Li, J., Sharkar, M.T.K., Xu, C.Y., Chen, B., Sun, J., Jing, D.,
803 and Xu, P.X. (2014). Eya1 interacts with Six2 and Myc to regulate expansion of the nephron
804 progenitor pool during nephrogenesis. Dev. Cell *31*, 434–447.
805 https://doi.org/10.1016/j.devcel.2014.10.015.

806 25. Liu, Z., Li, C., Xu, J., Lan, Y., Liu, H., Li, X., Maire, P., Wang, X., and Jiang, R. (2019). Crucial
807 and Overlapping Roles of Six1 and Six2 in Craniofacial Development. J. Dent. Res. *98*, 572–
808 579. https://doi.org/10.1177/0022034519835204.

809 26. Guan, J., Wang, D., Cao, W., Zhao, Y., Du, R., Yuan, H., Liu, Q., Lan, L., Zong, L., Yang, J., et
810 al. (2016). SIX2 haploinsufficiency causes conductive hearing loss with ptosis in humans. J.
811 Hum. Genet. *61*, 917–922. https://doi.org/10.1038/jhg.2016.86.

812 27. Caberlotto, E., Michel, V., Foucher, I., Bahloul, A., Goodyear, R.J., Pepermans, E., Michalski,
813 N., Perfettini, I., Alegria-Prévot, O., Chardenoux, S., et al. (2011). Usher type 1G protein sans
814 is a critical component of the tip-link complex, a structure controlling actin polymerization in
815 stereocilia. Proc. Natl. Acad. Sci. U. S. A. *108*, 5825–5830.
816 https://doi.org/10.1073/pnas.1017114108.

817 28. Kros, C.J., Marcotti, W., Van Netten, S.M., Self, T.J., Libby, R.T., Brown, S.D.M., Richardson,
818 G.P., and Steel, K.P. (2002). Reduced climbing and increased slipping adaptation in cochlear
819 hair cells of mice with Myo7a mutations. Nat. Neurosci. *5*, 41–47.
820 https://doi.org/10.1038/nn784.

821 29. Grati, M., and Kachar, B. (2011). Myosin VIIa and sans localization at stereocilia upper tip-link
822 density implicates these Usher syndrome proteins in mechanotransduction. Proc. Natl. Acad.
823 Sci. *108*, 11476–11481. https://doi.org/10.1073/pnas.1104161108.

824 30. Sato, O., Komatsu, S., Sakai, T., Tsukasaki, Y., Tanaka, R., Mizutani, T., Watanabe, T.M.,
825 Ikebe, R., and Ikebe, M. (2017). Human myosin VIIa is a very slow processive motor protein
826 on various cellular actin structures. J. Biol. Chem. *292*, 10950–10960.
827 https://doi.org/10.1074/jbc.M116.765966.

828 31. Wong, E.Y.M., Ahmed, M., and Xu, P.X. (2013). EYA1-SIX1 complex in neurosensory cell fate
829 induction in the mammalian inner ear. Hear. Res. *297*, 13–19.
830 https://doi.org/10.1016/j.heares.2012.09.009.

831 32. Xu, J., Li, J., Zhang, T., Jiang, H., Ramakrishnan, A., Fritzsch, B., Shen, L., and Xu, P.X.
832 (2021). Chromatin remodelers and lineage-specific factors interact to target enhancers to
833 establish proneurosensory fate within otic ectoderm. Proc. Natl. Acad. Sci. U. S. A. *118*.
834 https://doi.org/10.1073/pnas.2025196118.

835 33. Ahmed, M., Wong, E.Y.M., Sun, J., Xu, J., Wang, F., and Xu, P.X. (2012). Eya1-Six1
836 Interaction Is Sufficient to Induce Hair Cell Fate in the Cochlea by Activating Atoh1 Expression
837 in Cooperation with Sox2. Dev. Cell *22*, 377–390. https://doi.org/10.1016/j.devcel.2011.12.006.

838 34. Zhang, T., Xu, J., Maire, P., and Xu, P.X. (2017). Six1 is essential for differentiation and
839 patterning of the mammalian auditory sensory epithelium. PLoS Genet. *13*, 1–23.
840 https://doi.org/10.1371/journal.pgen.1006967.

841 35. Weiming Zheng, Li Huang, Zhu-Bo Wei, Derek Silvius, Bihui Tang, P.-X.X. (2003). The role of
842 Six1 in mammalian auditory system development. Development.
843 https://doi.org/10.1242/dev.00628.

844 36. N A Bermingham, B A Hassan, S D Price, M A Vollrath, N Ben-Arie, R A Eatock, H J Bellen, A
845 Lysakowski, H.Y.Z. (1999). Math1: an essential gene for the generation of inner ear hair cells.
846 *284*, 1837–1842.

847 37. Hertzano, R., Montcouquiol, M., Rashi-Elkeles, S., Elkon, R., Yücel, R., Frankel, W.N.,
848 Rechavi, G., Möröy, T., Friedman, T.B., Kelley, M.W., et al. (2004). Transcription profiling of
849 inner ears from Pou4f3ddl/ddl identifies Gfi1 as a target of the Pou4f3 deafness gene. Hum.
850 Mol. Genet. *13*, 2143–2153. https://doi.org/10.1093/hmg/ddh218.

851 38. Wallis, D., Hamblen, M., Zhou, Y., Venken, K.J.T., Schumacher, A., Leighton Grimes, H.,
852 Zoghbi, H.Y., Orkin, S.H., and Bellen, H.J. (2003). The zinc finger transcription factor Gfi1,
853 implicated in lymphomagenesis, is require for inner ear hair cell differentiation and survival.
854 Development *130*, 221–232. https://doi.org/10.1242/dev.00190.

855 39. Zhang, T., Xu, J., and Xu, P.X. (2021). Eya2 expression during mouse embryonic development
856 revealed by Eya2lacZ knockin reporter and homozygous mice show mild hearing loss. Dev.
857 Dyn. *250*, 1450–1462. https://doi.org/10.1002/dvdy.326.

858 40. Yang, H., Xie, X., Deng, M., Chen, X., and Gan, L. (2010). Generation and characterization of
859 Atoh1-Cre knock-in mouse line. Genesis *48*, 407–413. https://doi.org/10.1002/dvg.20633.

860 41. Caprara, G.A., Mecca, A.A., and Peng, A.W. (2020). Decades-old model of slow adaptation in
861 sensory hair cells is not supported in mammals. Sci. Adv. *6*, 1–13.
862 https://doi.org/10.1126/sciadv.abb4922.

863 42. Li, C., Liu, H., Hu, Y.C., Lan, Y., and Jiang, R. (2020). Generation and characterization of Six2
864 conditional mice. Genesis *58*. https://doi.org/10.1002/dvg.23365.

865 43. Caprara, G.A., Mecca, A.A., Wang, Y., Ricci, A.J., and Peng, A.W. (2019). Hair bundle
866 stimulation mode modifies manifestations of mechanotransduction adaptation. J. Neurosci. *39*,
867 9098–9106. https://doi.org/10.1523/JNEUROSCI.1408-19.2019.

868 44. Peng, A.W., Scharr, A.L., Caprara, G.A., Nettles, D., Steele, C.R., and Ricci, A.J. (2021). Fluid
869 Jet Stimulation of Auditory Hair Bundles Reveal Spatial Non-uniformities and Two Viscoelastic-
870 Like Mechanisms. Front. Cell Dev. Biol. *9*, 1–15. https://doi.org/10.3389/fcell.2021.725101.

871
872

Acknowledgement:

We thank Wenhao Xu and Daniel Grigsby at Genetically Engineered Murine Model Core (University of Virginia, RRID:SCR_025473) for generating mouse models used in this study. We thank Sijie Hao from Advanced Microscopy Facility (University of Virginia, RRID: SCR_018736) for the support of SEM imaging. We thank Ruliang Jiang (Cincinnati Children's Hospital Medical Center) for providing *Six2*$^{flox/flox}$ mice. We thank Maria Luisa S. Sequeira Lopez (University of Virginia) for providing the *Six2::cre-egfp* mice.

Funding source: J.B.S is supported by NIH grant RO1DC018842. Zeiss SEM of Advanced Microscopy Facility was supported by NIH SIG grant 1S10OD011966-01A1. The Titan Krios of Molecular Electron Microscopy Core is purchased with NIH grant SIG S10-RR025067.

Author contributions

Conceptualization: S.L., A. W.P., J.B. Shin; Methodology: S.L., S.J., Y.K., C.K., A.W.P., J.B. Shin; Experiments: S.L., S.J., Y.K., A.G., F.L.; Writing—review & editing: S.L., S.J., A. W.P., J.B. Shin; Supervision: U.K., A. W.P., J.B. Shin.